JOURNAL OF MATERIALS SCIENCE 20 (1985) 2303–2312

The microstructures of laser-alloyed Ni–Ta surface layers

C. W. DRAPER
A.T. & T. Technologies, Princeton, NJ 08540, USA

J. M. GIBSON, D. C. JACOBSON, J. M. POATE
A.T. & T. Bell Laboratories, Murray Hill, NJ 07974, USA

S. M. SHIN, J. M. RIGSBEE
Department of Metallurgy and Mining Engineering, University of Illinois at Urbana-Champaign, Urbana, IL 61801, USA

Evaporated thin tantalum films on single and polycrystalline nickel have been laser surface alloyed using either continuous-wave CO_2 or Q-switched Nd–YAG radiation. In the case of the continuous-wave laser, surface alloys contain amorphous tantalum-rich regions, intermediate polycrystalline bands of TaNi, and an underlying Ni(Ta) solid solution. In the Q-switched laser case, a much more laterally uniform amorphous phase with approximately equal atomic fractions of nickel and tantalum is found, with little evidence of polycrystalline intermetallics. *In situ* annealing with the electron beam of the microscope results in formation of microcrystallites, predominantly nickel.

1. Introduction

One of the newer and fastest growing areas in surface metallurgy research is in the use of directed-energy methods to produce surface alloys of chemical composition very different from their bulk substrates. Here we report the laser-induced alloying of tantalum films on nickel substrates. Thin alloy regions on nickel, prepared by laser surface alloying (LSA) and studied in our laboratory to date, include silver, palladium, tin, tantalum [1], gold [1, 2], cobalt and zirconium [3, 4]. The reasons for choosing nickel as a substrate were:

(a) the relative ease, compared to aluminium or copper, with which coupling could be accomplished using infrared laser sources,

(b) because of nickel's relatively low atomic number (an important factor in the use of Rutherford backscattering spectroscopy for analysis), and

(c) because of the diversity of phase-diagram behaviour exhibited by binary metal–Ni systems

Tantalum is amongst this group because of its very high melting point relative to nickel. In addition, the Ni–Ta system is a known compound-former and has been reported to be an inter-transition metal glass-former [5]. An earlier, preliminary report [1] on silver, gold, palladium, tin and tantalum surface alloys prepared by laser beams examined the chemical composition of the laser-mixed near surface regions. However, with the exception of Rutherford backscattering spectroscopy and channelling results, no microstructural information has been obtained. This report will detail the microstructures found in the case of tantalum films on nickel, laser-mixed with either cw CO_2 or Q-switched Nd–Yttrium Aluminium Garnet (YAG) lasers. We will show that both crystalline and amorphous phases are formed in the laser-mixed surface region, and that the formation of some of the phases can be understood in terms of the thermophysical and thermodynamic limitations imposed by the choice of tantalum and nickel.

2. Experimental procedure

Samples (19 mm^2, 0.64 mm thick) of commercial

0022–2461/85 $03.00 + .12

grade nickel 200 (> 99.5% Ni) were cut from rolled strip stock. The samples were cleaned successively in boiling trichloroethylene, methanol, high-purity water and spectroscopic grade methanol. Nickel single crystals were cut, lapped and electropolished to a mirror finish. Thin films of tantalum were vacuum deposited (electron-gun evaporator) at room temperature onto these nickel surfaces. Background vacuum conditions were 1×10^{-5} torr. Deposition rates were of the order of 10 nm min^{-1}. Film thicknesses were determined by Rutherford backscattering spectroscopy (RBS) [1] and ranged from 30 to 80 nm.

Laser mixing as accomplished with the continuous-wave (cw) CO_2 laser system is described fully and shown schematically in Fig. 1 of [6]. The Ni–Ta samples were mounted on a rotating wheel which, in turn, is mounted on a numerically controlled X–Y table. The combination of high speed of rotation (200 to 400 min^{-1}) and slow translation (V_X = 10 mm min^{-1}) results in overlapping of individual melt stripes, thus producing area coverage. The samples are mounted at a radial position (r = 9.5 cm) such that the transverse velocity in cm sec^{-1} is equal to the measured wheel revolutions per minute. Average laser powers of 0.5 to 1.1 kW were focused with a 6.35 cm ZnSe lens to spot sizes of approximately 0.1 mm diameter. The focusing lens was housed in a nozzle assembly. The use of argon as an inert "cover gas" (15 lb in^{-2} = 103 kPa) helped to suppress plasma formation at the sample surface, protect the lens from vaporized material and inhibit oxidation [6] of the sample surface.

The Q-switched Nd–YAG laser alloying system has been described previously [7]. Stationary samples are raster-scanned with laser pulses focused through a multi-element telecentric lens providing flat focusing over the sample field. Spot-to-spot and line-to-line overlap are adjusted for uniform area coverage. The pulse length and repetition rate were 130 nsec and 11 kHz respectively. The average laser power was 1 to 2 W and the gaussian spot size 30 to 40 μm.

The processing details given above for both cw and Q-switched irradiation may be used to estimate parameters used in theoretical heat-flow models such as those of Kear, Brienan and Greenwald [8] or Hsu, Chakravorty and Mehrabian [9]. Resolidification velocities for the Q-switched irradiation are of the order of 5 m sec^{-1}, and are several orders of magnitude greater than for the cw case.

Samples were prepared for transmission electron microscopy (TEM) by first chemically thinning from the back side in a solution of HNO_3–HCl–H_3PO_4–CH_3COOH (3:1:1:5 by volume) at 85° C for 25 min. The front surface was coated with protective lacquer and tape. The resulting 0.1 mm thick samples were electrolytically blanked into 3 mm diameter discs using a Struers Tenupol–2 jet-thinning apparatus. Before final thinning, samples were relacquered on the alloyed surface and a glass window was placed on the lacquer. This protected the alloyed surface while at the same time allowing the use of the auto-shutoff photocell. Final thinning was accomplished in a solution of CH_3COOH–$HClO_4$ (9.5:0.5 by volume) at 25° C. The laser-mixed samples were examined both before and after this preparation with both optical and scanning electron microscopy (SEM). In this manner, surface topographical features could be correlated with microstructural features found in TEM.

3. Results

3.1. cw CO_2 laser

Laser mixing of tantalum films on nickel results in a wavy surface topography and inhomogeneous distribution of tantalum. These features are seen qualitatively in the series of SEM micrographs and energy-dispersive X-ray analysis (EDAX) maps for tantalum in Fig. 1. This 65 nm Ta–Ni polycrystalline sample was laser-mixed with 0.5 kW of laser power at a transverse velocity of 400 cm sec^{-1}. In Figs. 1a and b melt puddles are seen running in a vertical direction, with a displacement (d_X) of 20 to 35 μm (see schematic diagram in Fig. 1c). It is quite evident in the tantalum distribution map of Fig. 1b that, relative to one another, the centre of the melt puddles are nickel-rich, whereas the melt edges are tantalum-rich. The SEM micrograph in Fig. 1a also shows evidence for the "rippled" surface topography which has been the object of considerable attention by other investigators [10–13]. In addition, there is in the SEM micrograph in Fig. 1a a random distribution of white specks, appearing almost like contaminant dust, which at the higher magnification in Fig. 1d are clearly resolvable "nodules", ranging in diameter from 0.1 to 5 μm, which the EDAX indicates are tantalum-rich relative to the surrounding matrix.

We expect that if the inhomogeneous tantalum distribution was due to incomplete laser

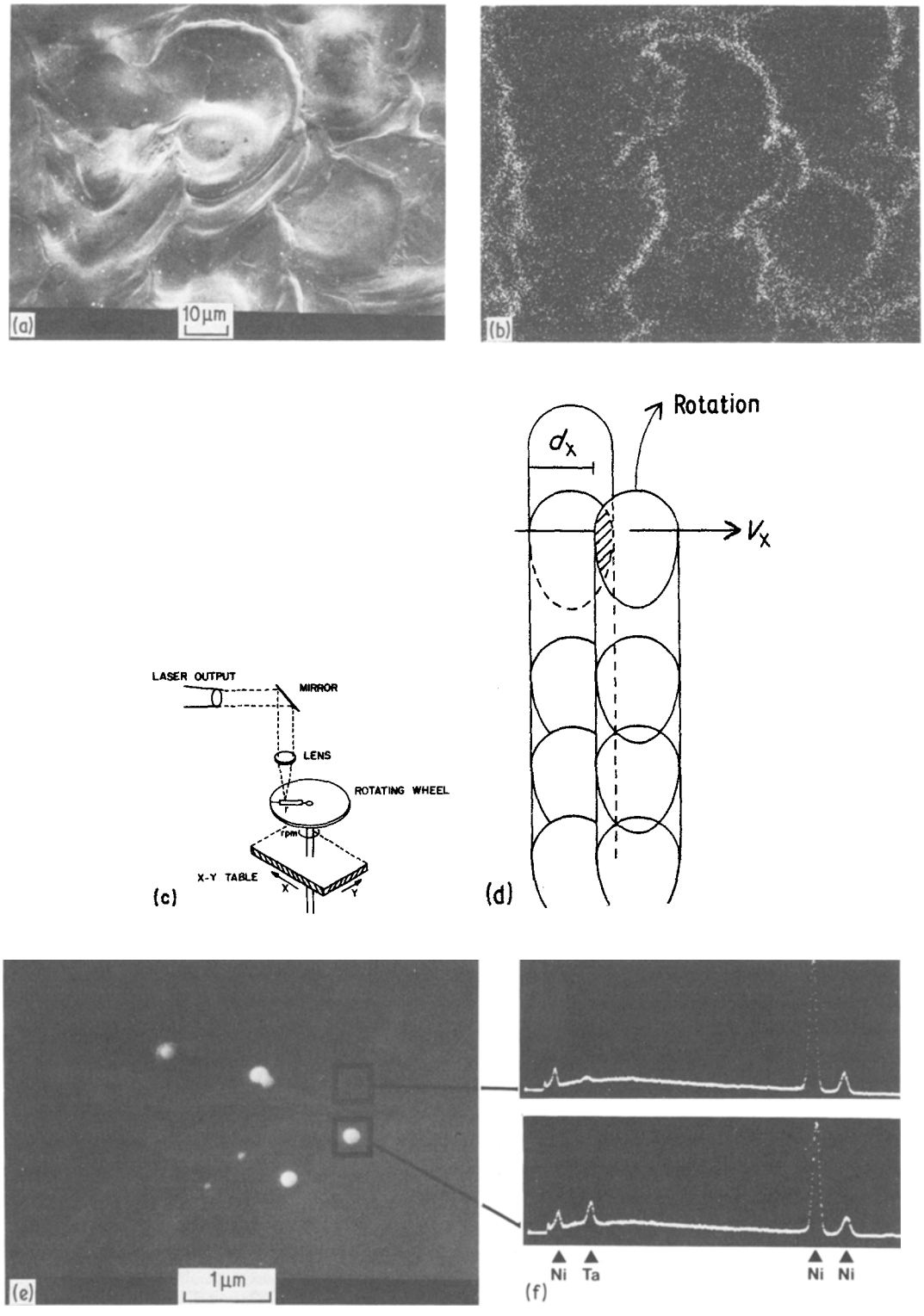

Figure 1 Scanning electron microcscopy surface-normal view of topographical features on laser-alloyed Ta–Ni. (a) SEM micrograph. (b) Energy-dispersive X-ray map for tantalum corresponding to micrograph. (c) Laser mixing with a cw CO_2 laser source. Ta–Ni samples are positioned on the rotating wheel at radial position r. (d) The combination of high rotation rate and slow translation, V_X, results in overlapping melt puddles for area coverage. (e) High-magnification SEM micrograph of some tantalum nodules and (f) the X-ray corresponding to the analysis areas indicated.

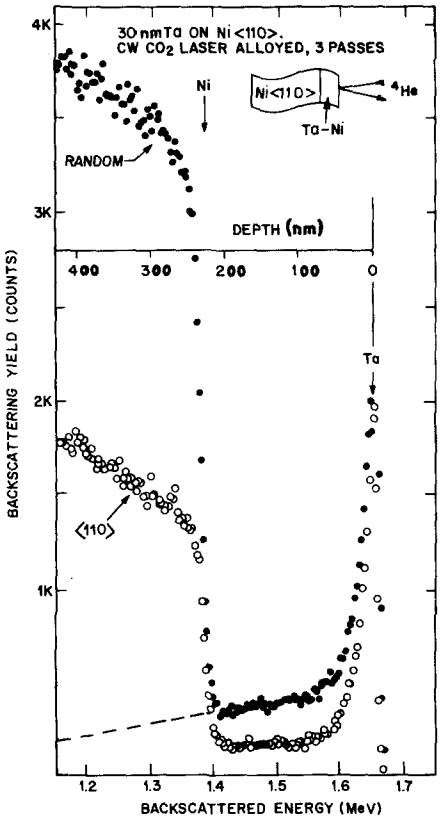

Figure 2 Rutherford backscattering spectra for 30 nm tantalum on single crystal nickel, laser-mixed with a cw CO_2 laser (0.5 kW, 200 cm sec^{-1}, three passes). Solid circles, random spectrum. Open circles, ⟨1 1 0⟩ aligned. Ni $\chi_{min} = 43\%$, Ta $\chi_{min} = 45\%$, original nickel crystal $\chi_{min} = 3\%$.

processing, repetitive exposure (repeating the scanning, melting, mixing and resolidification) would further homogenize the tantalum. Samples of 65 nm Ta–polycrystalline Ni, 80 nm Ta–polycrystalline Ni and 30 nm Ta–Ni ⟨1 1 0⟩ oriented single crystal were repetitively scanned (one, two, three and four passes) while processing with laser powers of 0.5 and 0.7 kW and transverse velocities of 200 and 400 cm sec^{-1}. Samples were examined with optical microscopy, SEM, EDAX, and RBS. We have found that repetitive processing results in the complete disappearance of the nodules, but that the tantalum-rich ridges are still present, and qualitatively in the same relative proportion even after four passes.

Fig. 2 presents random and ⟨1 1 0⟩ aligned He^+ backscattering yields for the 30 nm Ta–Ni ⟨1 1 0⟩ sample which has been LSA-processed three times. It is representative of results for regions processed between one and four times. The tantalum is found to be either located in a non-substitutional surface peak, or to be substitutionally alloyed into the nickel. The tantalum concentration is ~ 2 at % within the substitutional fraction, decreasing slowly with depth. If one extrapolates the substitutional fraction into the nickel by 1000 nm, then ~ 32% of the originally deposited tantalum is in solid solution after laser surface alloying, and ~ 28% of the deposited tantalum is tied up in the surface peak. This implies that alloying has occurred at low concentrations over a substantial depth (> 1000 nm) or that some loss of tantalum (roughly 40%) has occurred. The high χ_{min} for nickel (43%) after laser quenching is typical of the level of retained damage that we have observed in all our metallic surface-alloying studies with the cw CO_2 laser. One final point with regard to Fig. 2 is that although there is no channelling in the surface tantalum, there is channelling in the surface nickel. This is consistent with the laterally non-uniform composition depicted in Fig. 1.

Electro-polished thin samples of the laser-mixed tantalum on polycrystalline nickel were examined in a TEM operating at 200 kV. Electron-transparent areas were found in most of the distinct regions identified from optical microscopy and SEM. Only the large-diameter tantalum-rich nodules proved impossible to penetrate. Fig. 3a is a dark-field TEM micrograph from the edge of a melt puddle. This corresponds to one of the tantalum-rich ridges such as are seen in Figs. 1a and b. In this area of the specimen the thickness decreases from upper left to lower right, and therefore we are presented with a projected profile of the crystallography against depth from the original surface. Nearest the surface (upper left) a thin film of amorphous material is found, whose diffraction pattern is shown in Fig. 3b. We suspect that the amorphous material is a Ta–Ni glass. Examination of the identical region with SEM and EDAX confirms that the glassy regions are associated with the tantalum-rich fraction of the surface. Beneath this (centre) is a polycrystalline band, typical grain size of 100 nm, whose diffraction pattern is shown in Fig. 3c. Finally, in the lower right one sees substrate nickel grains, one of which is strongly diffracting in this picture. Many dislocations are visible in this grain. As previously mentioned, the original nickel substrates were prepared from commercial grade rolled strip stock, and thus

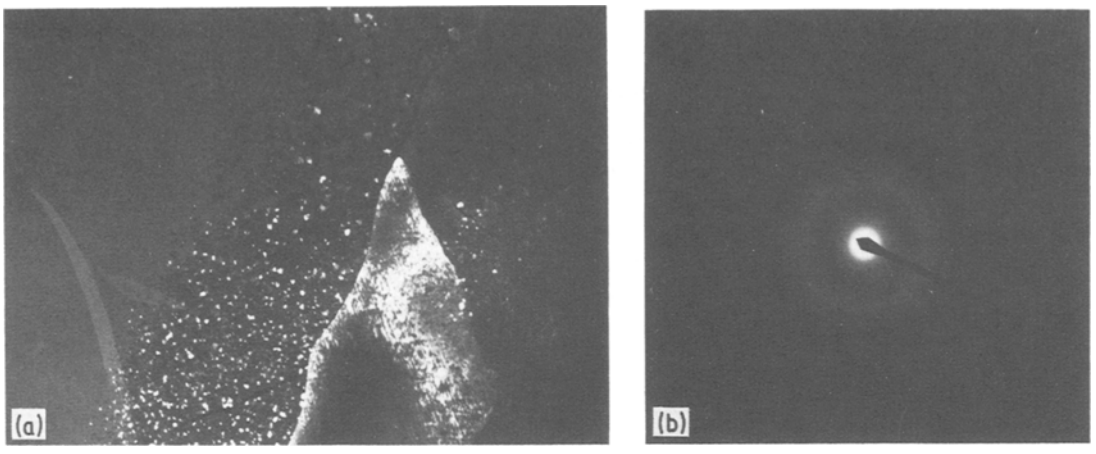

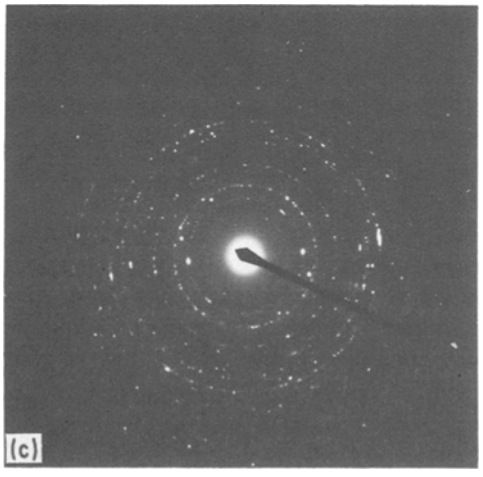

Figure 3 Transmission electron microscopy on thinned specimens. (a) Dark-field TEM micrograph from a tantalum-rich region. (b) Selected-area diffraction pattern from the featureless region (upper left) of the micrograph. (c) Selected-area diffraction pattern from a polycrystalline band associated with the tantalum-rich region. It is readily indexed as TaNi.

exhibited a grain size of several tens of micrometres and a high density of defects. Thus we cannot distinguish conclusively whether or not this grain had melted, and whether the associated defects are the result of laser quenching, but we suspect that they are.

Using the convenient single-crystal nickel diffraction spots as a standard we were able to index Fig. 3c, identifying the polycrystalline band as TaNi [14]. In the central portion of the melt puddles TEM analysis reveals no amorphous or polycrystalline tantalum-rich phases. In this area we expect, based on RBS and EDAX analysis, that a small quantity of tantalum (2 to 5%) is dissolved in the nickel grains.

3.2. Q-switched Nd–YAG laser

Laser alloying of tantalum films on nickel with 130 nsec Nd–YAG laser pulses results in a spatially more uniform tantalum distribution than that shown in Fig. 1 for the CO_2 laser. It is apparent, however, within the spatial resolution of EDAX mapping, that some spatial inhomogenieties in the tantalum content exist on the scale of the laser spot size ($< 50\,\mu m$). There is no evidence of "nodules" and the topography is considerably smoother than that produced by the CO_2 laser, which is to be expected since the melt depth and melt time are 1 to 2 orders of magnitude less.

RBS analysis of the Nd–YAG laser-alloyed tantalum in nickel indicates qualitatively similar features to those indicated in Fig. 2: the tantalum is found as both a surface tantalum-rich peak (though not so pronounced) and a substitutional fraction that extends down into the nickel. Since the melt depth is less than 1000 nm in the case of the Q-switched laser, the tantalum concentration in the near-surface region is greater for indentical starting film thicknesses when compared with the cw CO_2 laser-alloyed samples.

Examination of the microstructure and microchemistry of electron-transparent regions in the electropolished, as-laser-treated samples was done with a scanning and transmission electron microscope equipped for X-ray analysis. A thin, featureless film was present around the perimeter of the perforations in all examined areas. Electron diffraction analysis of this film (Fig 4b) showed it to be predominately amorphous. The low magnification dark-field image shown by Fig. 4a was formed by imaging with a portion

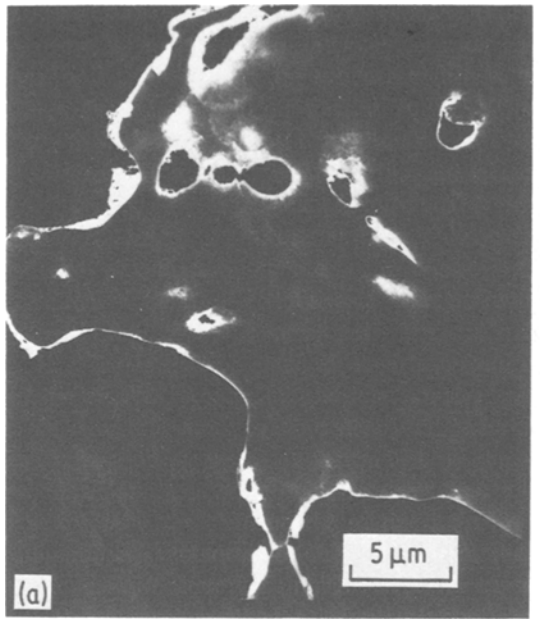

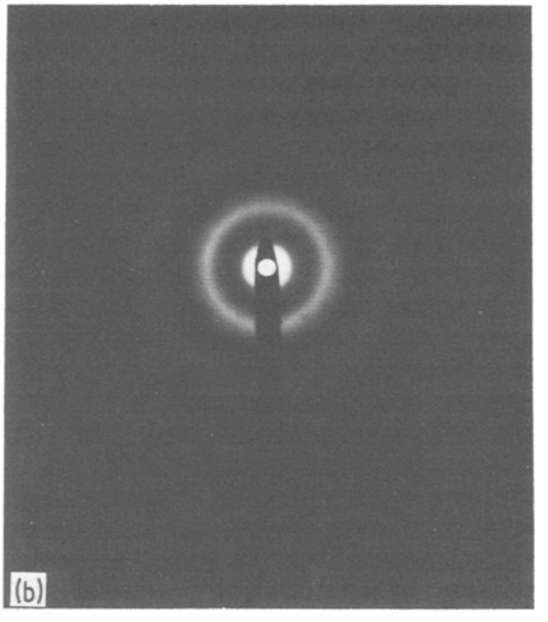

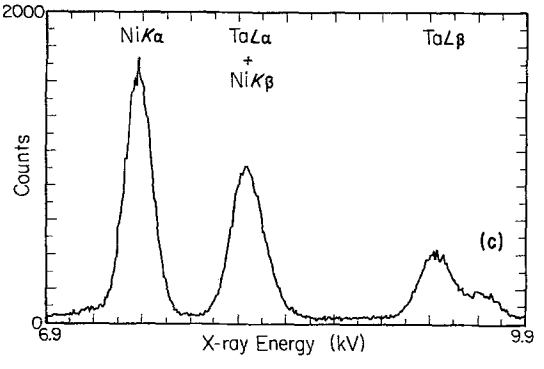

Figure 4 Characterization of the amorphous surface film. (a) Dark-field TEM micrograph showing continuous nature of the surface film. (b) Amorphous diffraction pattern from the surface film. (c) EDX spectra from the surface film.

of the stronger first amorphous diffraction ring. The apparent uniformity of coverage of the amorphous phase, as shown by the light regions around all perforation edges, suggests that the amorphous surface film is continuous. This is contrasted with the discontinuous surface film produced by CO_2 laser processing. Energy dispersive X-ray (EDX) analysis (without standards) of several amorphous film regions indicated approximately (50:50) equal atomic fractions of nickel and tantalum. Fig. 4c is a typical EDX spectrum from the amorphous surface film.

Occasionally, a small volume fraction of microcrystalline phase was found to be present in (or with) the amorphous surface film. Such an example is shown in Fig. 5a, a dark-field micrograph of the surface film. It is evident here that the volume fraction of crystalline phase increases as the nickel substrate is approached. This observation is consistent with the presence of an intermediate amorphous-plus-microcrystalline film between the fully amorphous surface film and the nickel substrate. Examination by electron diffraction (Fig. 5b) of the surface film region where the nickel substrate begins reveals that the microcrystalline phase is face-centred cubic (fcc). The overlapping in Fig. 5b of the diffraction rings from the microcrystalline phase and the diffraction spots from the nickel substrate indicates that the lattice parameter of the microcrystalline phase is essentially that of nickel. This would be consistent with the initial precipitation of nickel from the laser-melted region and, after a critical tantalum concentration is reached, the later formation of the amorphous Ni–Ta alloy. Some evidence was also found by electron diffraction that a small amount of body-centred cubic (bcc) phase also forms, with a lattice parameter very close to that of tantalum. This is seen in Fig. 5b as a very weak third ring. The expected stronger ⟨1 1 0⟩ bcc diffraction ring is not visible since it overlaps with the ⟨1 1 1⟩ fcc ring.

Fig. 5c shows the effects of *in situ* electron-beam heating for 20 min (temperature unknown) on the degree of microcrystallinity, for the same region and dark-field imaging conditions as in

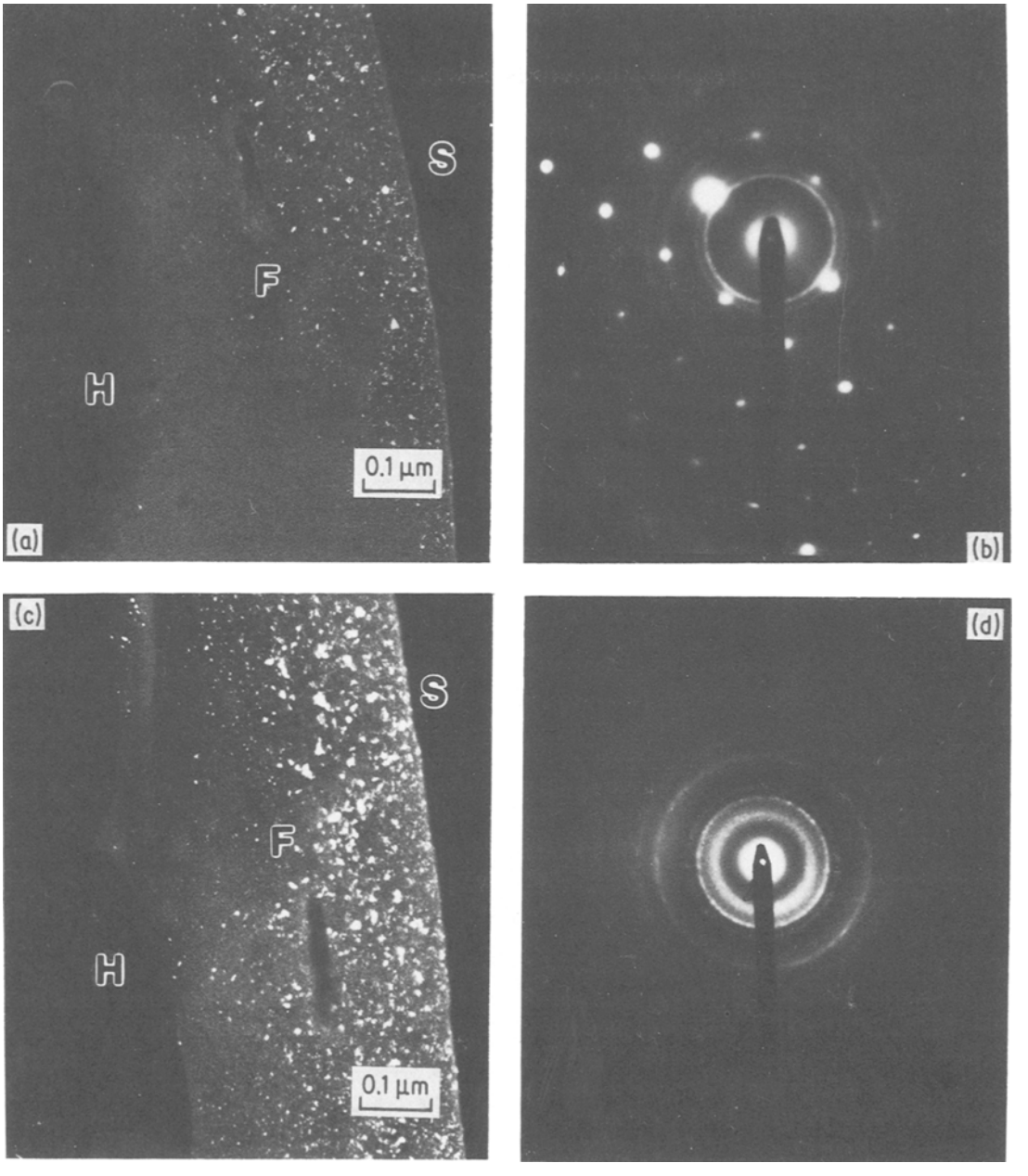

Figure 5 Amorphous and microcrystalline phases. (a) Typical microcrystallinity prior to heating. Dark-field micrograph; **H** indicates electropolished hole, **F** indicates surface film and **S** indicates thick nickel substrate. (b) Selected-area electron diffraction pattern from substrate–surface film overlap region. (c) Dark-field micrograph showing increased microcrystallinity after heating. (d) Selected-area electron diffraction pattern from surface film showing amorphous and FCC microcrystalline phases.

Fig. 5a. Clearly the volume fraction and average grain size of the microcrystalline phase have both increased. In support of the previously described multilayer surface-layer concept, it is still evident that the microcrystallinity increases as the substrate is approached. Fig. 5d is an electron diffraction pattern from the surface film (no substrate contribution). This diffraction pattern shows both the diffuse inner ring from the remaining amorphous matrix and the sharper fcc rings from the microcrystalline phase. In almost all instances the crystalline phase was fcc. However, in several

but relatively very few areas we saw a ring pattern similar to that found for the CO_2 laser-processed material.

4. Discussion

We shall first consider the tantalum-rich nodules seen in Figs. 1a and d. We believe they are formed from pieces of the original tantalum film which detaches during laser processing. Their spherical nature clearly shows that they have been molten. They have probably been ejected as liquid and resolidified, either in the high-pressure argon environment or upon contact with an area of cold substrate outside the narrowly defined melt zone. We have already pointed out that the tantalum-rich nodules seen in Figs. 1a and d completely disappear upon repetitive processing. There are two possible explanations for this observation. The first is that upon repeated melting the nodules are dissolved into the melt, thus adding to the average alloyed tantalum concentration. A second explanation is that upon further irradiation the nodules, which are in poor thermal contact with the surface on which they reside, evaporate before the underlying material melts. Alloying element loss is known to occur by several mechansims during LSA processing [3, 15], but in the case of CO_2 laser alloying it is difficult to quantify because the deep melting and uncertain role of convective mixing makes it difficult to account (with EDX or RBS) for all the incorporated alloyed species. Regardless of which of the two explanations above is correct, the point remains that the tantalum-rich nodules are not a reproducible microstructural feature resulting from resolidification of the melt, but are peculiar to a certain set of laser-processing conditions. Furthermore the nodules can be eliminated by repetitive processing.

As was pointed out in Section 1, one of the reasons that the Ta–Ni system was chosen for investigation was because glass formation has previously been reported. Ruhl *et al.* [16] and Giessen *et al.* [5] report producing amorphous Ni_xTa_{1-x} foils ($0.25 < x < 0.7$) by splat quenching (SQ) techniques. Schafer and Menzel [17] have used vapour quenching (VQ) under ultra-high vacuum conditions to produce thin amorphous Ni_xTa_{1-x} films in the range $0.2 < x < 0.55$. They further classify these VQ amorphous films into one of two categories (metglass or solid-amorphous) based on the number, location and relative intensity of the diffuse rings found in the electron diffraction patterns. The electron diffraction patterns in Figs. 3 to 5 are not similar to the reported electron diffraction patterns of either the SQ or VQ Ni–Ta glasses. Specifically, the patterns previously reported [5, 16, 17] appear more ordered than ours. However, it is well known that the degree of ordering in glasses is very dependent on the exact preparation conditions. Schafer and Menzel [17] further point out that gas-doped amorphous tantalum films (using both argon and nitrogen) have radically different electron diffraction patterns. In view of these differences in preparation methods it is probably no surprise, therefore, that there is little similarity between the electron diffraction patterns observed for SQ, VQ and LSA-produced Ni–Ta glasses.

In the case of the CO_2 laser-alloyed specimens, the TEM and selected-area electron diffraction analysis of the tantalum-rich regions of several samples at numerous perforation sites reveal an intimate spatial interrelationship between the glassy material and the polycrystalline TaNi phase. The Nd–YAG laser-alloyed glassy material contrasts with that produced by the CO_2 laser by being continuous across the surface. Polycrystalline precipitates are not generally found in the glass; but when found, their location is nearer the underlying nickel substrate than the surface. Two of the more important factors influencing inter-transition metal glass formation are the quench rate and the relative composition. In addition, the two factors are interrelated in that the glass-forming composition range usually increases with higher quench rates. Therefore, in preparation methods (such as LSA), where there are spatial variations in both the relative composition and quench rates, one might expect the glass-forming criteria to be met non-uniformly.

These two points, compositional and quench-rate dependence, are the object of a recent investigation by Yatsuga and Massalski [18]. They have recently published a detailed investigation into the formation of amorphous Pd–Si–Cu regions when laser-melting crystalline alloy surfaces with both cw CO_2 and pulsed ruby lasers. They deduce a strong correlation between the presence of a very fine crystalline "intermediate zone" (between original crystalline substrate and the laser-induced amorphous regions) and resolidification interface velocity. Models like those mentioned earlier [8, 9] show that the resolidification interface

velocity starts out by being slow and rapidly increases. As the moving liquid–solid interface picks up speed a critical velocity is reached, and Yatsuga and Massalski [18] show that a clearly demarcated glass–crystalline border is predicted and is observed. In our particular case, where surface alloying results in spatial chemical non-homogeneity, in addition to the changing resolidification velocities such a correlation would be much more difficult to attempt.

It would appear that the most likely reason for the spatial correlation between the glassy Ta–Ni and the microcrystalline phase(s) is that, upon recrystallization of the tantalum-rich melt regions, either compositional or quenching factors are such that first microcrystalline and then amorphous material is formed. There are, however, other possible explanations for this behaviour. One is that the glassy regions is stabilized by gas-doping and that, since the uppermost liquid will be preferentially exposed to the argon (CO_2 laser case) and to N_2 and O_2 (Nd–YAG case), the glassy region is formed only nearest the surface. Although the irradiation times and associated melt times are rather short, there is still ample time for the melt to be affected by the ambient gas environment. As has been pointed out in our laser-alloying work on Hf–Ni [4, 6] and Cu–Zr [19], when metals with a high affinity for ambient gases are involved, even melting and resolidification on the nanosecond time scale can be affected by the surrounding gas. However, unlike Cu–Zr [19] laser-alloyed amorphous layers, which upon thermal annealing reveal the stabilizing oxygen by formation of ZrO_2 microcrystallites, we have no indication from our *in situ* annealing of Ta–Ni for such stabilization.

Another alternative explanation is that the microcrystalline phases have been formed upon partial decomposition of the Ta–Ni glasses during temperature cycling associated with the heat-affected zones, and with the repetitive nature of the processing used to produce surface area by the overlapping of individual melt events. Thermal annealing at temperatures above 600° C for the SQ glass [16] leads to formation of TaNi and $TaNi_2$. VQ films are reported [20] to crystallize at temperatures above 400° C. Temperatures below the melting point, but easily at or in excess of the T_g values reported in [16] and [20], are very likely to be reached during the repetitive heat cycling. Observations like this have been reported by Pfeiffer and Hock [21] in preparation of CuZr glassy surfaces from bulk crystalline alloys by laser quenching with pulsed Nd–YAG lasers. However, in both our CO_2 laser and Q-switched Nd–YAG laser-alloyed amorphous layers, the microcrystallites are not found in those areas where the thermal cycling would reach the greatest temperature and for the longest period of time, but rather nearer to the maximum melt-depth interface.

5. Conclusions

Intermixing of tantalum films on nickel substrates with the cw CO_2 laser results in a nonuniform tantalum distribution, both laterally and in depth. The tantalum-rich regions are found on the surface at the edges of melt stripes, and are not removed by repetitive laser processing. The microstructure of the tantalum-rich regions has been identified by TEM to contain both a glassy tantalum-rich phase and the crystalline phase TaNi. The nickel-rich regions making up most of the quenched volume contain 2 to 5 at% Ta in solution. The Q-switched Nd–YAG laser produces a glassy Ta–Ni surface layer which, in contrast to that formed by the CO_2 laser, is continuous across the surface. Very small quantities of fcc and bcc precipitates are occasionally found in the amorphous material, nearer to the nickel substrate than to the surface. *In situ* thermal annealing induced by the electron beam has been used to induce crystallization of fcc nickel in the amorphous layer.

Acknowledgements

The technical assistance of Mr R. J. Crisci in the thinning preparation of samples for TEM is greatly appreciated. Two authors (SMS and JMR) gratefully acknowledge the financial support of the Materials Science Division, US Department of Energy, under contract DE–AC02–76ER01 198. We would also like to acknowledge the use of the facilities at the Centre for Microanalysis of Materials located in the Materials Research Laboratory of the University of Illinois.

References

1. C. W. DRAPER, C. W. PREECE, D. C. JACOBSON, L. BUENE and J. M. POATE, "Laser and Electron Beam Processing of Materials", edited by C. W. White and P. S. Peercy (Academic, New York, 1980) p. 721.
2. C. W. DRAPER, L. S. MEYER, L. BUENE, D. C. JACOBSON and J. M. POATE, *Appl. Surf. Sci.* 7 (1981) 276.

3. C. W. DRAPER, F. J. A. DEN BROEDER, D. C. JACOBSON, E. N. KAUFMANN and J. M. VANDENBERG, "Laser and Electron Beam Interactions with Solids", edited by B. R. Appleton and G. K. Celler (North Holland, New York, 1982) p. 419.
4. E. N. KAUFMANN, L. BUENE, M. L. MCDONALD, J. KOTTHAUS, K. FREITAG, R. VIANDEN and C. W. DRAPER, *Nucl. Instrum. Meth.* **209/210** (1983) 427.
5. B. C. GIESSEN, M. MADHARA, D. E. POLK and J. VANDER SANDE, *Mater. Sci. Eng.* **23** (1976) 145.
6. C. W. DRAPER, E. N. KAUFMANN and L. BUENE, *Surf. Interface Anal.* **4** (1982) 8.
7. G. K. CELLER, J. M. POATE and L. C. KIMERLING, *Appl. Phys. Lett.* **32** (1978) 464.
8. B. H. KEAR, E. M. BRIENAN and L. E. GREENWALD, *Met. Technol.* **6** (1979) 121.
9. S. C. HSU, S. CHAKRAVORTY and R. MEHRABIAN, *Met. Trans.* **9B** (1978) 221.
10. S. M. COPELY, D. BECK, O. ESQUIVEL and M. BASS, "Laser–Solid Interactions and Laser Processing–1978", edited by S. D. Ferris, H. J. Leamy and J. M. Poate (Conference Proceedings No. 50, American Institute of Physics, New York, 1979) p. 161.
11. S. L. NARASIMHAN, S. M. COPELY, E. W. VAN STRYLAND and M. BASS, *Met. Trans.* **10A** (1979) 654.
12. T. R. ANTHONY and H. E. CLINE, *J. Appl. Phys.* **48** (1977) 3888.
13. P. MOORE, C. KIM and L. S. WEINMAN, "Laser–Solid Interactions and Laser Processing–1978, edited by S. D. Ferris, H. J. Leamy and J. M. Poate (Conference Proceedings No. 50, American Institute of Physics, New York, 1979) p. 221.
14. P. I. KRIPYAKEVICH, E. I. GLADYSHEVSKII and E. N. PYLAEVA, *Soviet Phys.–Cryst.* 7 (1962) 165 (ASTM index).
15. C. DRAPER, *J. Metals* **34** (1982) 24.
16. R. C. RUH, B. C. GIESSEN, M. COHEN and N. J. GRANT, *Acta. Metall.* **15** (1967) 1693.
17. A. SCHAFER and G. MENZEL, *Thin Solid Films* **52** (1978) 11.
18. S. YATSUYA and T. B. MASSALSKI, *Mater. Sci. Eng.* **54** (1982) 101.
19. F. J. A. DEN BROEDER, J. M. VANDENBERG and C. W. DRAPER, *Thin Solid Films* **111** (1984) 43.
20. A. SCHAFER and G. MENZEL, *Electrocompon. Sci. Technol.* **4** (1977) 29.
21. I. PFEIFFER and S. HOCK, *Z. Metallkde.* **72** (1981) 36.

Received 17 July
and accepted 31 July 1984